Quim. Nova, Vol. 43, No. 4, 391-398, 2020 http://dx.doi.org/10.21577/0100-4042.20170507

Artigo

$Ce_{\alpha}Mn_{1-\alpha}O_2$ CATALYSTS SUPPORTED OVER γ-Al_2O_3 PREPARED BY MODIFIED REDOX-COPRECIPITATION METHODS FOR n-HEXANE COMBUSTION

Jesus Rojas Quispe[a], Romulo Cruz[a], Rosario Sun Kou[b] and Gino Picasso[a,*]

[a]Laboratory of Physical Chemistry Research, Faculty of Sciences, National University of Engineering, Tupac Amaru 210 Av., Rimac, Lima, Peru

[b]Departament of Sciences, Section Chemistry, Pontifical Catholic University of Peru, Av. Universitaria 1801, San-Miguel, Lima 32, Peru

Recebido em 24/06/2019; aceito em 14/01/2020; publicado na web em 31/03/2020

A series of $Ce_{\alpha}Mn_{1-\alpha}O_2$ catalysts supported on γ-alumina with various molar concentrations of Ce (α, from 0 to 0.90) was synthesized by coprecipitation, applying two different precipitating agents, namely, sodium hydroxide (method 1) and sodium carbonate (method 2), with the use of sodium permanganate as a redox agent for precipitation. XRD profiles of the supported samples revealed the predominant abundance of a typical fluorite crystalline structure. TPR thermograms of supported samples were displaced towards lower temperatures with increasing Mn concentration, in contrast with the bulk samples. The supported Ce-Mn samples exhibited a greater performance in n-hexane elimination than did the corresponding simple oxides. The sample $Ce_{0.33}Mn_{0.67}O_2$ obtained by method 2 presented the best activity, probably due to the enrichment of Ce^{4+}, Mn^{3+} and Mn^{4+} surface species, an excess of superficial oxygen species and an easy reducibility as well as the lowest apparent activation energy.

Keywords: VOC; n-hexane; Ce-Mn; modified-precipitation; alumina.

INTRODUCTION

The world is increasingly aware of climate change and global warming, and the signatories of the twenty-first session of the Conference of the Parties (COP 2015, or the "Paris Accord") have committed to intensify efforts to control carbon dioxide emissions. These reductions in emissions should limit a global temperature increase this century to less than two degrees above preindustrial levels. However, while important, carbon dioxide emissions are not the only large-scale pollution problem resulting from human activity. Volatile organic compounds (VOCs) form a group of chemicals responsible for photochemical smog, and many of them are known to be carcinogenic and teratogenic.[1] Increasing regulations to control VOC levels, especially in work and home environments, demand the best technologies to control their release.[2] Specifically promising is catalytic technology that allows VOCs to be eliminated at temperatures much lower than incineration combustion, making the formation of nitrogen oxides negligible.[3]

The application of noble metals as catalysts in VOC combustion is usually limited by their high cost, scarcity and sensitivity at high temperatures. Metal oxides are promising alternatives due to their high activity and resistance to poisoning.[3] In particular, the manganese oxides have been well studied in VOC combustion due to the chemical characteristic of manganese to the structure of multivalent oxides and their important ability to collect bulk oxygen.[4-8] The formation of MnO_x species has shown high performance in the total combustion of different model organic molecules including o-xylene,[9] methane,[10] ethyl methyl ketone,[11,12] 1,2-dichlorobenzene,[13] n-hexane,[14] toluene[15,16] and ethanol,[17] among others.

n-Hexane is a solvent commonly used in the chemical industry, but its application in the manufacturing of drugs has been restrained due to its ongoing toxicity. OSHA[18] and NIOSH[19] have regulated its emission to the atmosphere as a hazard, setting an exposure limit of 500 ppm for 8 h. In previous works, some catalysts based on $CeMnO_x$ and $CeZrO_y$ were prepared in a membrane configuration[11] and in a packed-bed reactor with bulk samples[14] for the elimination of n-hexane. The catalytic tests revealed a strong influence of the Mn^{4+} and Ce^{4+} species over the surface, which had the ability of storing surface oxygen through redox reactions following a Langmuir-Hinshelwood mechanism. While redox processes clearly played a substantial role in the catalytic performance, some questions related to the preparation variables and their influence on the formation of the active phase require deeper discussion as is suggested by some authors.[20] With this aim, some factors were taken into consideration in this work, namely, the dispersion effect using a conventional γ-alumina support and the effect of preparation variables proposed via modifying precipitation agents and calcination conditions as well as their influence on the catalytic behavior of alumina-supported Ce-Mn oxides in the abatement of n-hexane.

EXPERIMENTAL

Catalyst preparation

A series of $Ce_{\alpha}Mn_{1-\alpha}O_2$ catalysts was synthesized modifying the relative molar concentration of cerium from α=0.33 to 0.9 by coprecipitation using different precipitating agents and redox conditions. Prior to the preparation of the catalysts, the γ-Al_2O_3 support (99.9%, SIGMA-ALDRICH) was heated to 135 °C in a closed balloon reactor under vacuum to eliminate any remaining water, which was verified by the differences in weights before and after the thermal treatment. Moreover, the alumina-supported simple oxides were prepared for α=0 (CeO_2) and for α=1 (MnO_x) following each method of preparation, which were the following:

Method 1

In method 1, the catalysts were prepared by suspension-coprecipitation with a redox reaction step using a solution of 0.2 mol L^{-1} NaOH (MERCK) as a precipitating agent. This solution was added at 0.5 mL min^{-1} to a beaker containing a suspension of

*e-mail: gpicasso@uni.edu.pe

γ-Al_2O_3 with a 0.5 mol L^{-1} solution of metallic precursors of a mixture of Ce and Mn nitrates and potassium permanganate with a molar ratio (m/m) of 5:3:2, respectively, at 60 °C under constant stirring to achieve a pH up to 10.5.[21,22] The solid was aged for 2 h and washed 5 times using deionized water to avoid the presence of the remaining alkali ions. Finally, the solid was dried at 110 °C for 12 h and calcined for 6 h at 500 °C under air atmosphere (heating rate=5 °C/min). The mechanism of preparation corresponds to the mixed precipitation-redox route developed over the support γ-Al_2O_3:[23]

$$MnO_4^- + 3e^- + 2H_2O \rightarrow MnO_2\downarrow + 4OH^- \quad (1)$$
$$Mn^{2+} + 4OH^- \rightarrow MnO_2\downarrow + 2e^- + 2H_2O \quad (2)$$
$$Ce^{3+} + 4OH^- \rightarrow CeO_2\downarrow + e^- + 2H_2O \quad (3)$$

The composition of the catalyst was achieved by the controlled dose of the different starting solutions[23] through the following equations:

$$3 \text{ mol MnVII} = 2 \text{ mol MnII} + \text{mol CeIII} \quad (a)$$
$$(\text{mol MnVII} + \text{mol MnII}) / \text{mol CeIII} = (\text{mol Mn /mol Ce}) \quad (b)$$
$$\text{mol MnVII} + \text{mol MnII} + \text{mol CeIII} = 1 \quad (c)$$

The equations correspond to the (a) charge balance, (b) molar balance and (c) compositional balance of the catalyst.

Method 2

This method was similar to method 1, but using a solution of 0.2 mol L^{-1} Na_2CO_3 as a precipitating agent,[24,25] which was introduced to a solution of Ce and Mn nitrate precursors with potassium permanganate with the molar ratio of 5:3:2, respectively, at 50 °C, increasing the pH level to 10.5 under vigorous stirring. Then, the solid was aged for 2 h and washed until removal of Na^+. The final solid was dried at 110 °C for 12 h, heated at a heating rate of 5 °C/min and finally calcined at 500 °C for 6 h in air. The mechanistic route of the process was the following:

$$MnO_4^- + 3e^- + 2H_2O \rightarrow MnO_2(s) + 4OH^- \quad (4)$$
$$Mn^{2+} + CO_3^{2-} \rightarrow MnCO_3(s) \quad (5)$$
$$2Ce^{3+} + 3CO_3^{2-} \rightarrow Ce_2(CO_3)_3(s) \quad (6)$$
$$(x/2)\, Ce_2(CO_3)_3(s) + (1-x)\, MnCO_3(s) \rightarrow Ce_xMn_{1-x}O_2\,(s) + CO_2(g) \quad (7)$$

Table 1 lists the alumina-supported mixed catalysts ($Ce_\alpha Mn_{1-\alpha}O_2$) prepared in this work. The mixed oxide supported catalysts were denoted as CMx-y, in which "x" is assigned to α, i.e., it corresponds to the nominal metallic ratio Ce/(Ce+Mn), and "y" indicates the method of preparation. The simple oxide supported samples were designated as C-x or M-x, in which "x" corresponds to the method of preparation. The samples were distributed into three groups in order to compare the method of preparation and the metal composition for the catalysts prepared by methods 1 and 2 due to their higher performances in n-hexane elimination.

Table 1. Alumina-supported mixed catalysts based on $Ce_\alpha Mn_{1-\alpha}O_2$ (40% metallic charge) prepared in this work

Catalyst	Method of preparation	Ce/Mn ratio	S_{BET} (m^2/g)
Comparative method			
CM0.5-1	1	1	174
CM0.5-2	2	1	182
γ-Al_2O_3	-	-	170
Comparative Ce/(Ce+ Mn) ratio - Method 1			
CM0.33-1	1	0.5	169
CM0.5-1	1	1	174
CM0.67-1	1	2	236
CM0.9-1	1	9	211
C-1	1	-	157
M-1	1	-	124
Comparative Ce/(Ce+ Mn) ratio - Method 2			
CM0.33-2	2	0.5	129
CM0.5-2	2	1	182
CM0.67-2	2	2	177
C-2	2	-	168
M-2	2	-	132

Characterization of catalysts

The crystal structures of the catalysts were studied by X-ray diffraction (XRD). The characterization was performed using a RIGAKU Miniflex diffractometer, whose operating parameters were as follows: 15 mA, 30 kV, Cu Kα radiation (λ = 1.5418 Å), Ni filter, and range of angle scanning from 5 to 80° (step size = 0.10° and step time = 2.5 s). The identification of the crystal phases was made by application of the PDF2 database from ICDD. The Scherrer equation was used to estimate the average crystallite sizes from the peak of the highest intensity in the diffractograms, and the Gauss function was used to fit the selected diffraction peaks.

The texture of the catalysts was analyzed by the technique of sorption of N_2, performed at liquid nitrogen temperature with a Micromeritics GEMINI VII-2390t system. Before the analysis, the catalysts were pretreated in a He stream at 250 °C for 2 h. The BET method and the t-plot procedure were applied to evaluate the total specific surface area and the microporous area of catalyst, respectively. The method of BJH (Barrett, Joyner, and Halenda) from the adsorption at a P/P_0 near 0.98 was used to measure the total pore volume as well as the pore size distribution and the mean pore size (using the desorption branch of the isotherm).

The redox properties of the catalysts were studied by temperature-programmed reduction (H_2-TPR) and temperature-programmed desorption of oxygen (O_2-TPD), performed with a MICROMERITICS CHEMISORB 2720 Pulse Chemisorption System. As a rule, the TPR tests were carried out in a U-tube quartz reactor in which 25 mg of the sample was deposited under a stream of 10% H_2/He and warmed from the room temperature to 900 °C at a heating rate of 10 °C min^{-1}. A standard quantity of Ag_2O was used to calibrate the H_2-consumption. The estimation of oxidation state of Mn has been made considering only the MnO as the oxide present at the end of all the TPR tests. The O_2-TPD tests were performed in a reactor using 100 mg of the sample pretreated with a helium purge (25 mL min^{-1}) for 30 minutes at 200 °C and followed by an injection of a flow of 10% O_2 in He (25 mL min^{-1}) for 30 minutes at 500 °C. Then, under a gas stream of 10% He in N_2, the catalysts were cooled to room temperature. Finally, another helium purge (25 mL min^{-1}) was performed to remove O_2 molecules, heating the furnace at a rate of 10 °C min^{-1} from 30 °C to 850 °C. A thermal conductivity detector (TCD) was employed to quantify the loss of O_2.

The chemical surface analysis of samples was evaluated by X-ray photoelectron spectroscopy (XPS). The spectrometer used was VG 200 R with a 120 W-powered X-ray source of Al Kα1 (hν = 1486.6 eV). The XPS spectra were recorded on small Inox holders with a vacuum system, heating in the presence of a residual

pressure of 10^{-6} mbar at 573 K for 5 h. Furthermore, the spectra were collected at 200 eV pass energy for survey spectra and 50 eV pass energy for narrow scans. Afterwards, the catalysts were introduced into the analysis chamber in which a residual pressure of 5.10^{-9} mbar was inserted. High-resolution spectra of Ce 3d, Mn 2p, C 1s and O 1s and a survey spectrum were acquired for each catalyst, each with multiple scans in order to achieve good signal-to-noise ratios. The binding energies of Cu 2p3/2 (932.6 eV) and Au 4f7/2 (84.0 eV) were used as a calibration reference of the spectrometer. The binding energy of the C 1s signal of adventitious carbon at 284.8 eV was used to correct possible generated charge effects of spectra of the catalysts. The fitting of the experimental spectra with ±0.1 eV of precision of the binding energy values was achieved through a combination of Gaussian and Lorentzian lines (G/L = 90/10), subtracting the sigmoidal background. The most intensity ratios, normalized by atomic sensitivity factors, were used to display the atomic ratios of samples.

Catalytic tests

The experimental setup was detailed in a previous work.[14] The reaction equipment involved a quartz packed-bed reactor operating at atmospheric pressure, whose dimensions were 9 mm internal diameter and 600 mm height. The main experimental parameters of the testing such as the gas WHSV (weight hourly space velocity) and particle size were tuned to underestimate the internal and external diffusion effects. The temperature of the reaction tests was recorded by a thermocouple inserted into the catalyst bed where 100 mg of sample was mixed with 200 mg of Pyrex glass beads to control hot spots, all deposited over a quartz frit. The feed section of the experimental equipment included two gas flows: synthetic air (Praxair, 99.99%) used as diluent gas and the other gas being air saturated with n-hexane (MERCK, 99.9%), formed from n-hexane saturators at ice temperature and regulated pressure. The experimental conditions used for all the catalytic tests were 100 cm^3 STP.min^{-1} for the total flow rate, 2000 ppmV for the initial VOC concentration and 80 h^{-1} for the WHSV. The reaction products of the catalytic tests were monitored by a gas chromatograph (GC-HP450) equipped with a column HP-INNOWax of 30 m × 0.32 mm i.d. and connected to an FID detector for VOC recording and a methanizer to follow the CO_2 emissions. The conversion was measured as VOCs consumed (%) after the reaction. In all the catalytic tests, only complete combustion species were obtained. The 50% and 95% conversion temperatures in the ignition curves ($T_{50\%}$ and $T_{95\%}$, respectively) were used for the evaluation of the catalytic activities of the samples.

RESULTS AND DISCUSSION

Textural analysis and X-ray diffraction (XRD)

From Table 1, an increase in cerium composition of mixed samples led to an increased specific surface area, in accordance with similar works.[14,17] The isotherms of alumina-supported mixed oxides catalysis prepared by method 1 were of type II, as was observed for the samples CM0.5-1 and CM0.67-1 with 40% metallic charge (Figure 1).

Furthermore, all the adsorption isotherms of the samples prepared by method 2 were also classified as type II, corresponding to macroporous material. All samples showed a type H3 hysteresis loops, corresponding to the formation of slit-shaped pores. In addition, an increase in metallic charge leads to an increased specific surface area (data not shown). Taking into account that the supported samples with a metallic load of 40% (no matter the method of preparation) allowed species with higher specific BET surface areas to be obtained and achieved better performance in the combustion of n-hexane, this optimal metallic charge was studied in more detail in further tests.

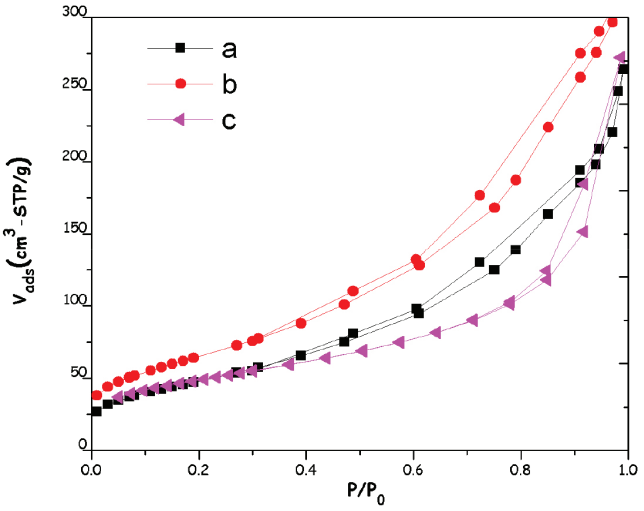

Figure 1. *Isotherms of supported mixed catalysts prepared by method 1 with 40% metallic charge and with different metallic molar proportions, a: CM0.50-1, b: CM0.67-1, c: γ-Al_2O_3*

The diffractogram of the mixed oxide samples with 40% metallic charge compared with their simple oxide counterparts is shown in Figure 2. As is observed, the simple cerium oxides showed distinguishable separated defined peaks corresponding to the fluorite phase whose crystallinity decreased slightly with decreasing metallic charge over the support, probably due to the better dispersion achieved in the metal-rich samples. The diffractogram of manganese presented peaks attributed to Mn oxide, with a major presence of Mn_3O_4 (PDF2 # 24e0734), very similar to the results obtained in previous works.[11,14] The alumina-supported mixed samples presented a profile similar to the fluorite phase corresponding to alumina-supported ceria with 40% charge, but with wider peaks and lower sizes of crystallites (Table 2), showing a higher dispersion of the metallic phase over the surface of the support. No peaks assigned to MnO_x were observed, i.e., the addition of any quantity of cerium to manganese completely affects the initial multiphase structure of MnO_x, very similar to that observed in bulk conditions.[14] In this case, a small displacement of the peaks addressed to the high diffraction angles is observed, most likely because of the introduction of Mn^{n+} species with lower ratio in the lattice (Mn^{2+} = 0.83 Å, Mn^{3+} = 0.645 Å and Mn^{4+} = 0.53 Å) to the Ce^{4+} sites (1.01 Å). The formation of only one structure suggests the formation of mixed phases, which appeared to be clarified due to the observed lowering of the cell parameter of supported mixed oxides with respect to the corresponding pure ceria (Table 2). Regarding supported samples prepared by method 1 and method 2 (Figure 1S), those with low cerium content (<0.5) presented the same phases. The XRD profiles of the manganese-supported samples prepared by method 1 differ from those of method 2 because the majority phase is now monoclinic Mn_5O_8 (PDF2 # 39e1218) and cubic Mn_2O_3 (PDF2 # 73e1826) instead of tetragonal Mn_3O_4 (PDF2 # 24e0734), as has also been observed by some authors.[26]

Temperature programmed reduction (TPR)

The characterization by H_2-TPR analysis was applied to the alumina-supported mixed oxide samples prepared by different methods. The support γ-Al_2O_3 presented a consumption of H_2 at reduction temperatures over than 1000 °C; consequently, the reduction peaks observed in the H_2-TPR thermograms are exclusively owing to

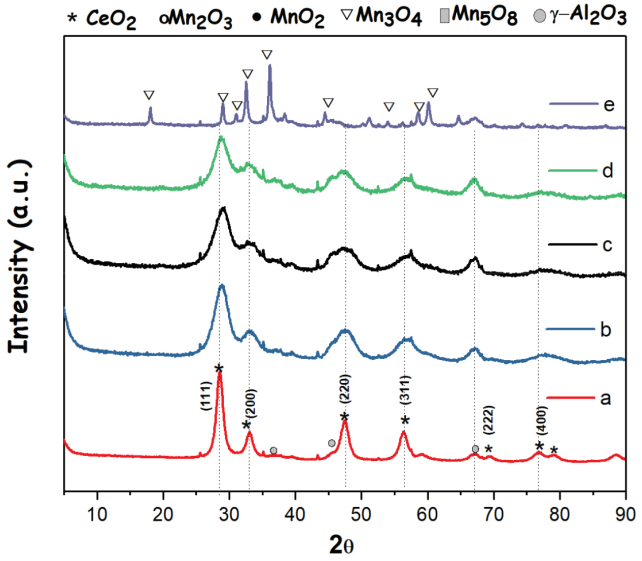

Figure 2. *XRD patterns of the supported mixed samples with 40% metallic charge prepared by method 2, a: C-2, b: CM0.67-2, c: CM0.50-2, d: CM0.33-2 and e: M-2*

Table 2. Comparison of structural parameters studied from XRD analysis for simple and mixed oxide supported samples, prepared by method 2

Catalyst	Metallic charge over γ-Al_2O_3 (%)[a]	Crystal-lite size (nm)[b]	Cell parameter (Å)[c]
M-2	40	-	-
CM0.33-2	40	3.7	5.36
CM0.50-2	40	3.1	5.33
CM0.67-2	40	3.1	5.36
C-2	40	5.0	5.50

[a]From the components during the preparation. [b]Obtained from the Debye-Scherrer equation, plane (111). [c]Calculated from the plane (111).

the reduction of the metallic species. In the profile corresponding to C-2 (40%) presented in Figure 3, two reduction peaks are depicted, at 516 °C and 690 °C, which are consistent with the reduction of nonstoichiometric superficial Ce^{4+} species (tetrahedrally coordinated with the oxygen atoms) and the reduction of Ce^{4+} to Ce^{3+} in the bulk phase, respectively.[17] The first peak was shifted to the higher temperatures with respect to that observed in the bulk phase in previous work,[14] probably due to the interaction with the γ-Al_2O_3 support. The reduction of Ce^{4+} to Ce^{3+} (bulk) is typical of the fluorite crystalline structure,[14] which confirms the XRD diffractograms, as already discussed.

The H_2-TPR profile of M-2 (40%) shown in Figure 3 exhibits three reduction peaks positioned at temperatures near 320, 360 and 443 °C, ascribed to the successive reduction steps from MnO_2 to MnO as reported by some authors:[27,28]

$$MnO_2 \rightarrow \alpha\text{-}Mn_2O_3 \rightarrow Mn_3O_4 \rightarrow MnO \quad (8)$$

As discussed in previous work,[14] the stoichiometry of bulk manganese oxide calculated from the consumption of H_2 of the corresponding profile in Figure 3 is in good agreement with the presence of Mn_2O_3, Mn_3O_4 and MnO_2. In this case, the reduction temperatures were displaced towards higher temperatures than those observed in the bulk phase,[14] which is compatible with the influence of the metal-support interactions. All these data are in good agreement with the XRD diffractograms of Figure 2.

The H_2-TPR thermograms of a series of catalysts CM0.5 (40%) prepared by methods 1 and 2 are presented in Figure 3. All the profiles are very similar, no matter the method of preparation, and exhibit one broad defined peak, situated at 240-250 °C, and a shoulder at 410-415 °C. According to some authors,[29] the first peak could be assigned to the reduction of superficial Mn^{4+} species situated over Ce lattice positions, and the second peak could be attributed to the reduction of Mn^{3+} species. The profile of the CM0.5-2 (40%) differs from the others due to the presence of a broader peak at the first reduction temperature, probably due to the major consumption of H_2, revealing an easier reducibility caused by the better positions of Mn^{4+} species over the surface. Moreover, in this sample, a minor peak situated at 411 °C confirmed that the Mn_2O_3 particles are quickly transformed, remaining only as the Mn^{4+} species, exhibiting a broader peak, most likely owing to a much higher dispersion of the active phase.[30]

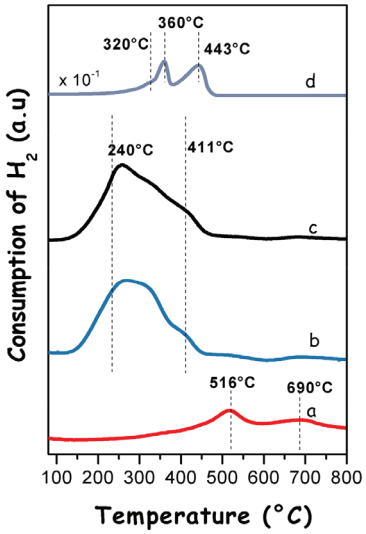

Figure 3. *H_2-TPR profiles of alumina-supported mixed samples prepared by different methods and with a 40% metallic charge, a: C-2, b: CM0.5-2, c: CM0.5-1, d: M-2*

The influence of metal composition on the reduction properties of the catalysts from method 2 (40%) is depicted in Figure 2S. The thermograms were shifted to lower temperatures with decreasing Ce/Mn ratio due to the enrichment in Mn. The higher area of the first peak in the TPR, corresponding to both CM0.5-2 and CM0.33-2, reveals the major consumption of H_2 in relation to the predominant concentration of Mn^{4+} reduced to Mn^{3+} species. The best reducibility in the catalysts CM0.33-2 led to a better performance in the total oxidation of n-hexane, so it was studied in greater detail. The results of the O_2-TPD analysis (Figure 3S) showed that the labile species of oxygen are in the highest concentration in the mixed samples and that method 2 led to catalysts with a higher quantity of labile oxygen, which was desorbed at low temperatures.

X-ray photoelectron spectroscopy (XPS)

Table 3 shows the normalized absolute areas from the XPS spectrum (in CPS.eV) of a series of CM0.33 (40%) alumina-supported catalysts synthesized by methods 1, 2 as well as the corresponding catalysts prepared by method 2, CM-0.33-2 (30%), CM-0.33-2 (20%) and the simple oxides C-1 (40%), M-1 (40%), prepared by method 1. To determine the atomic percentages, the atomic ratios were normalized using the corresponding sensitivity factors.

The signals corresponding to the Mn $2p^{3/2}$ XPS spectrum

Table 3. Normalized absolute areas of a series of CM0.33 alumina-supported catalysts prepared by methods 1 and 2 and the corresponding simple oxides prepared by method 1

Catalyst	Normalized absolute areas (CPS.eV)					Ce/(Ce+Mn) XPS
	C 1s	O 1s	Ce 3d	Mn 2p	Al 2p	
CM0.33-2 (20%)	7059	35198	305	450	19343	0.40
	11.32%	56.45%	0.49%	0.72%	31.02%	
CM0.33-2 (30%)	8625	38340	606	628	20305	0.49
	12.59%	55.97%	0.88%	0.92%	29.64%	
CM0.33-2 (40%)	8189	34812	425	520	18187	0.45
	13.18%	56.03%	0.68%	0.84%	29.27%	
CM0.33-1 (40%)	11326	23299	1780	1271	7920	0.58
	24.84%	51.10%	3.90%	2.79%	17.37%	
C-1 (40%)	10725	23326	1619	0	7714	1.00
	24.72%	53.77%	3.73%	0.00%	17.78%	
M-1 (40%)	7216	32203	0	3400	14772	0
	12.53%	55.92%	0.00%	5.90%	25.65%	

(Figure 4) of a series of catalysts were deconvoluted by a fitting process after subtraction of the background, using XPS commercial software. The compounds MnO, $ZnMn_2O_4$ and $MgNiMnO_4$ were used as a references of the binding energies and FWHM values of the Mn^{2+} (641.1 eV, 2 eV), Mn^{3+} (641.9 eV, 2.7 eV) and Mn^{4+} (644.0 eV, 4 eV).[31-33] The Mn 2p core level in pure MnO_x (M-1, 40%) allowed finding a Mn cation distribution expressed as a percentage ratio $[Mn^{2+}]$: $[Mn^{3+}]$: $[Mn^{4+}]$ equal to 19.9: 53.8: 26.2, from which it was inferred that Mn^{3+} and Mn^{4+} were the majority species (Table 3). Similar results were obtained for the samples of a series of CM-0.33 catalysts prepared by different methods (Figure 4). As is observed, in the sample CM0.33-2, prepared by method 2, Mn^{4+} species are in a greater proportion than in the samples prepared by method 1. Additionally, the low surface percentage of Mn over the support (Table 3) indicates a good dispersion of the active phase. In the case of the CM0.33 series catalysts prepared by method 2 and with different metallic loads, as is observed in Table 4, the total percentage of Mn^{4+} and Mn^{3+} increases as the metallic load increases.

The O 1s spectra of the mixed oxides (Figure 5) were deconvoluted into two contributions, namely, surface-adsorbed oxygen in the BE range of 531 to 531.6 eV, related to defect surface oxygen species such as O_2^{2-} or O^- (usually denoted as O_β), and the corresponding BE range of 528.9–530 eV, usually ascribed to lattice oxygen (O_α).[34-37] During the deconvolution of the different samples, the FWHM value was maintained constant in the range of ±0.1 eV. The O 1s spectrum of C-1 (40%) presented two maxima centered at 529.5 and 531.6 eV, attributed to lattice oxygen and surface oxygen, respectively; meanwhile, the O 1s core level of oxygen of M-1 (40%) was situated at 530.2 and 531.5 eV. For C-1 (40%), the percentage of superficial oxygen abundance was 82.2, and for M-1 (40%), 95.3.

According to Table 4, sample CM0.33-2 (40%) presented a higher relative enrichment of adsorbed oxygen (100%) than did the other analogous samples prepared by method 1 (82.1%) (Figure 5). This enrichment in surface oxygen in alumina-supported mixed samples of Ce-Mn is in accordance with the data discussed by Arena *et al.*,[30] in which the formation of very reactive electrophilic oxygen species was ascribed to the "Mn←O" electron-transfer processes. Moreover, the increase in the metal load over the support from 20 to 40% had no significant effect on the percentage of surface oxygen, as is observed in Table 4 with the CM0.33 sample series prepared by method 2.

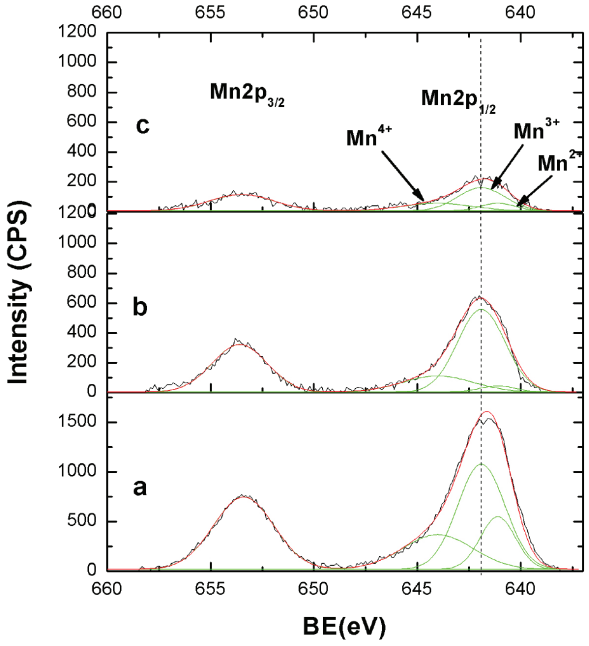

Figure 4. *Mn 2p3/2 XPS spectra: deconvoluted peaks of samples prepared by different methods of preparation. Peaks are centered at 641.1 eV (Mn^{2+}), 641.9 eV (Mn^{3+}) and 644 eV (Mn^{4+}), a: M-1, b: CM0.33-1, c: CM0.33-2*

In all samples, the Ce 3d spectra, deconvoluted (Figure 4S) for sample CM0.33-2, presented multiplets v and u, according to the notation of Burroughs *et al.*[38] These multiplets corresponded to the spin-orbital division $3d^{5/2}$ and $3d^{3/2}$ of the 3d internal level, which was approximately 18.6 eV in accordance with other investigations.[39] Moreover, the FWHM was fixed as a constant value during the deconvolution of each multiplet peak. Each spin-orbital division could be composed of three peaks in the case of CeO_2 and only two peaks in the case of Ce_2O_3.[40] Therefore, it is necessary to analyze 10 peaks if taking into account both spin-orbital divisions. This analysis was made by a detailed adjustment of the data to Gaussian curves.[40-44] As is shown in Table 4, the sample CM0.33-2 (40%) prepared by method 2 achieved the lowest value of total Ce concentration compared to the rest of the samples, CM0.33-1 (40%). This observation could indicate a good dispersion of the active phase over the support. Moreover,

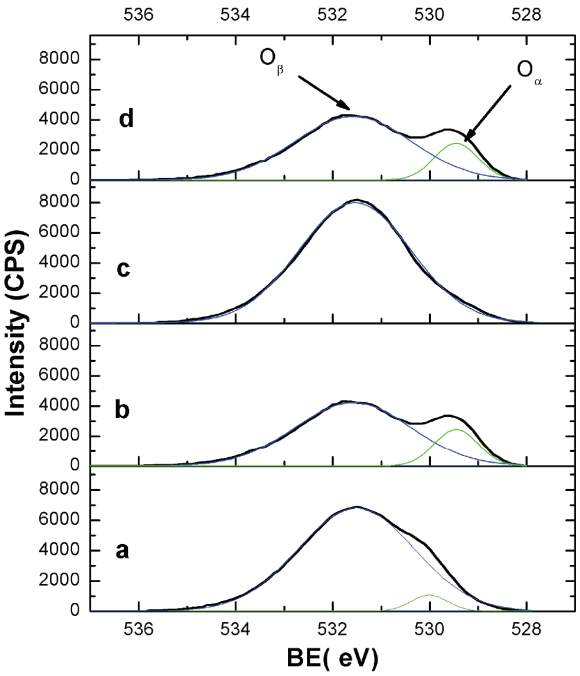

Figure 5. *O 2p XPS spectra: deconvoluted peaks with a 40% metallic charge for different methods of preparation, a: M-1, b: CM0.33-1, c: CM0.33-2 and d: C-1*

the percentage of Ce^{4+} in all samples ranged from 81.6 to 86.5. Most likely, according to some authors, the content of Ce^{3+} reported in this work is due to the reduction of Ce^{4+} that takes place during the XPS analysis.

Catalytic activity of the catalysts in the combustion of n-hexane

The combustion of n-hexane performed without a catalyst indicated the absence of activity at the working temperatures. The following experimental variables were considered in all the catalytic tests: method of preparation, the metallic load of the active phase over the support and the composition of metal loading over the support.

Influence of the metallic load

The activity of alumina-supported Ce-Mn prepared with different metallic loads and with an equimolar molar composition is shown in Figure 6. As is shown, the mixed oxide samples with 40% metallic load presented more activity than did the samples with 20 and 50%, all prepared by method 2. This behavior is probably related to the higher presence of Mn^{3+} and Mn^{4+} species as shown in the XPS analysis (Figure 4) and its higher specific surface area relative to that of the other equimolar mixed samples with the same metallic load (Table 1). The reactive oxygen species (O^-, OH^-, O_2^{2-}, and O_2^-) greatly favor the combustion of volatile organic compounds.[8] The presence of these species is evidenced by the BE value of the oxygen atom in these samples (Table 4).

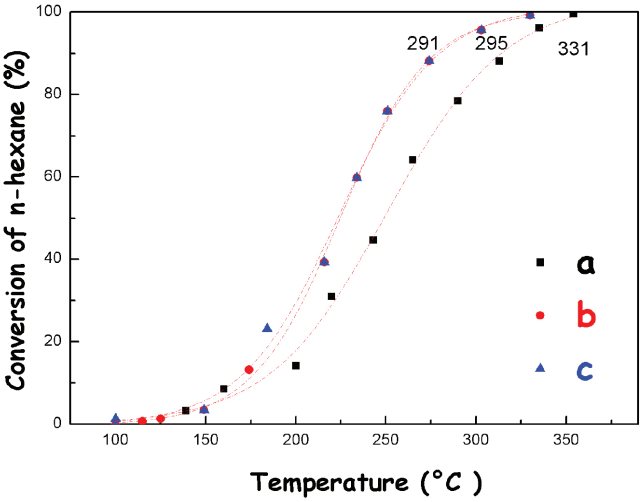

Figure 6. *Ignition curves of mixed oxide alumina-supported catalysts with different amounts of metallic charge prepared by method 2, a: CM0.50-2 (20%), b: CM0.50-2 (40%), c: CM0.50-2 (50%)*

Influence of the method of preparation

The activity of the Ce-Mn alumina-supported samples prepared by different methods and with 40% metallic charge is shown in Figure 5S. As is observed, all the mixed oxides samples present more activity than did the simple oxide supported samples. The activity

Table 4. Percentage of O, Ce and Mn species of a series of CM0.33 alumina-supported catalysts prepared by methods 1 and 2 and the corresponding simple oxides prepared by method 1

Catalyst	O 1s	O 1s	Ce 3d	Ce 3d	Mn 2p	Mn 2p	Mn 2p
	BE(eV)	BE(eV)	-	-	BE(eV)	BE(eV)	BE(eV)
	% Lattice oxygen	% Surface oxygen	% Ce^{3+}	% Ce^{4+}	% Mn^{2+}	% Mn^{3+}	% Mn^{4+}
CM0.33-2 (20%)	0.0	100.0	16.5	83.5	26.5	31.0	42.5
	-	531.4		-	641.1	641.9	644.0
CM0.33-2 (30%)	1.8	98.2	17.7	82.3	19.9	52.5	27.6
	529.1	531.5	-	-	641.1	641.9	644.0
CM0.33-2 (40%)	0.0	100.0	14.3	85.7	14.1	57.5	28.3
	-	531.5	-	-	641.1	641.9	644.0
CM0.33-1 (40%)	17.9	82.1	18.4	81.6	4.1	74.4	21.5
	529.5	531.6	-	-	641.1	641.9	644.0
C-1 (40%)	17.8	82.2	16.5	83.5	0.0	0.0	0.0
	529.5	531.6	-	-	-	-	-
M-1 (40%)	4.7	95.3	0.0	0.0	19.9	53.8	26.2
	530.0	531.5	-	-	641.1	641.9	644.0

decreases in the following order: CM0.50-2 > CM0.50-1 > M-1 > C-1. It could be inferred that the coprecipitation-redox method of preparation with carbonate allowed the formation and development of the active and selective sites. This behavior of the samples with the best catalytic activity could be assigned to the higher abundance of Mn^{4+} species, surface oxygen, abundance of labile oxygen species and a higher reducibility.

Effect of metallic composition of the catalysts prepared by method 2

Since the catalysts prepared by method 2 presented a better activity, some further test experiments were performed to study the effect of the metal composition (Figure 7). As was observed, the catalyst CM0.33-2 showed a higher activity than that of the catalysts CM0.5-2 and CM0.67-2. The H_2-TPR thermograms of the sample CM0.33-2 (Figure 2S) presented higher reducibility relative to that of the other samples. XPS spectra confirmed the highest presence of electrophilic oxygen in this sample, usually responsible of the total combustion of n-hexane.

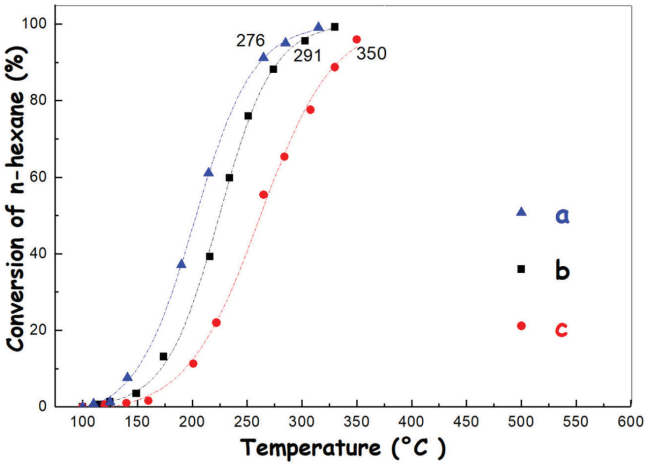

Figure 7. *Influence of metal composition of the catalysts with a 40% metallic charge on the activity in the combustion of n-hexane, a: CM0.33-2, b: CM0.50-2 and c: CM0.67-2*

The Arrhenius plots allowed determination of the values of Ea for the catalysts prepared with different metal compositions (Figure 8).

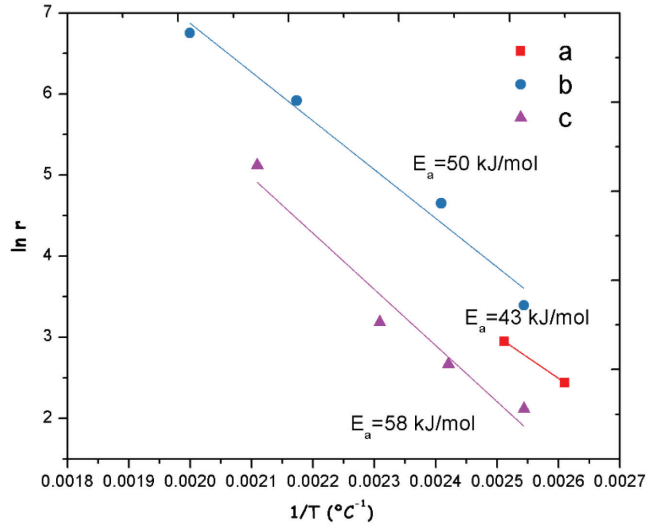

Figure 8. *Arrhenius plots used to compare the activity of the catalyst prepared by method 2 with a 40% metallic charge, a: CM0.33-2, b: CM0.50-2 and c: CM0.67-2*

The lower activation energy is usually related with the activity of the catalysts and the rate velocity of the reaction, so a better catalyst is expected. The lower the E_a value is (43 kJ/mol), the easier the hexane can be oxidized, and this value was achieved for the sample CM0.33-2 with 40% metallic load. The high catalytic activity can be associated with a better reducibility, high content of Mn^{4+} and Mn^{3+} species as well as the best synergistic interaction between Ce and Mn, achieved through the method of preparation with sodium carbonate.

CONCLUSIONS

The supported Ce-Mn samples showed better activities in n-hexane combustion than did the simple oxides. The sample $Ce_{0.33}Mn_{0.67}O_2$ prepared by method 2 showed the highest activity, probably due to the enrichment of Mn^{3+} and Mn^{4+} surface species as well as the relatively favorable reducibility related to the corresponding supported single oxides. The alumina-supported Ce-Mn sample prepared by suspension-coprecipitation with the redox reaction with potassium permanganate and Na_2CO_3 used as a precipitating agent appeared to have the best performance. The sample $Ce_{0.33}Mn_{0.67}O_2$ precipitated with sodium carbonate exhibited the highest activity for n-hexane combustion, probably due to the better Ce-Mn interaction between the surface species Ce^{4+}, Mn^{3+} and Mn^{4+} with the contribution of the metal-support interaction. This sample also showed the highest reducibility and an abundance of superficial oxygen species, which favored the total combustion of n-hexane, revealing the synergistic effect of the Ce-Mn metal interaction.

SUPPLEMENTARY MATERIAL

Figures 1S-5S are freely available at http://quimicanova.sbq.org.br, in PDF format.

ACKNOWLEDGMENTS

The authors want to express their sincerest gratitude to the Research Management Office of National University of Engineering of Lima-Peru (OGI) for the financial support for this work and Dr. Silvia Irusta from Universidad de Zaragoza by the XPS measurements and assisting spectra identification. R. C. wishes to acknowledge FONDECYT (Convenio n°208-2015-FONDECYT) for his Master scholarship.

REFERENCES

1. Ahmad, W.; Noor, T.; Zeeshan, M.; *Catal. Commun.* **2017**, *89*, 19.
2. Tang, W. X.; Wu, X.; Li, S.; Li, W.; Chen, Y.; *Catal. Commun.* **2014**, *56*, 134.
3. Spivey, J. J.; *Ind. Eng. Chem. Res.* **1987**, *26*, 2165.
4. Jirátová, K.; Kovanda, F.; Balabánová, J.; Kšírová, P.; *Catal. Today* **2018**, *304*, 165.
5. Hu, J.; Li, W. B.; Liu, R. F.; *Catal. Today* **2018**, *314*, 147.
6. Hinokuma, S.; Shimanoe, H.; Kawabata, Y.; Kiritoshi, S.; Araki, K.; Machida, M.; *Catal. Commun.* **2018**, *105*, 48.
7. Morales, M. R.; Yeste, M. P.; Vidal, H.; Gatica, J. M.; Cadus, L. E.; *Fuel* **2017**, *208*, 637.
8. Tang, W.; Li, W.; Li, D.; Liu, G.; Wu, X.; Chen, Y.; *Catal. Lett.* **2014**, *144*, 1900.
9. Wu, Y.; Shi, S.; Yuan, S.; Bai, T.; Xing, S.; *Appl. Surf. Sci.* **2019**, *479*, 1262.
10. Wang, X.; Yiu, L.; Zhang, Y.; Zhang, T.; Chang, H.; Zhang, Y.; Jiang, L.; *Appl. Catal., B* **2018**, *229*, 52.

11. Picasso, G.; Gutiérrez, M.; Pina, M. P.; Herguido, J.; *Chem. Eng. J.* **2007**, *126*, 119.
12. Lerner, E. C.; Peluso, M. A.; Sambeth, J.; Thomas, H.; *J. Rare Earths* **2016**, *34*, 675.
13. Tang, A.; Xu, L.; Yang, X.; Jia, Y.; Zhang, Y.; *Catal. Commun.* **2016**, *82*, 41.
14. Picasso, G.; Cruz, R.; Sun Kou, M. R.; *Mater. Res. Bull.* **2015**, *70*, 621.
15. Lu, H.; Kong, X.; Huang, H.; Zhou, Y.; Chen, Y.; *J. Environ. Sci.* **2015**, *32*, 102.
16. Morales, M. R.; Barbero, B. P.; Cadús, L. E.; *Catal. Lett.* **2011**, *141*, 1598.
17. Matějová, L.; Topka, P.; Kaluža, L.; Pitkäaho, S.; Ojala, S.; Gaálová, J.; Keiski, R. L.; *Appl. Catal., B* **2013**, *54*, 142.
18. https://www.osha.gov/dts/chemicalsampling/data/CH_245400.html, accessed on March 2020.
19. https://www.cdc.gov/niosh/npg/npgd0322.html, accesed on March 2020.
20. Li, T. Y.; Chiang, S. J.; Liaw, B. J.; Chen, Y. Z; *Appl. Catal., B* **2011**, *103*, 143.
21. Xingfu, T.; Yonggang, L.; Xiumin, H.; Yide, X.; Huaqing, Z.; Jianguo, W.; Wenjie, S.; *Appl. Catal., B* **2006**, *62*, 265.
22. Liu, X.; Lu, J.; Qian, K.; Huang, W.; Luo, M. A.; *J. Rare Earths* **2009**, *27*, 418.
23. Arena, F.; Trunfio, G.; Negro, J.; Spadaro, L.; *Mater. Res. Bull.* **2008**, *43*, 539.
24. Meng, M.; Tu, Y.; Ding, T.; Sun, Z.; Zhang, L; *Int. J. Hydrogen Energy* **2011**, *36*, 9139.
25. Li, J. G.; Ikegami, T.; Wang, Y.; Mori, T.; *J. Am. Ceram. Soc.* **2002**, *85*, 2376.
26. Qi, K.; Xie, J.; Fang, D.; Liu, X.; Gong, P. F.; Li, F.; He, F.; *Mater. Chem. Phys.* **2018**, *209*, 10.
27. Terribile, D.; Trovarelli, A.; Leitenburg, C.; Primavera, A.; Dolcetti, G.; *Catal. Today* **1999**, *47*, 133.
28. Gil, A.; Gandía, L. M.; Korili, S. A.; *Appl. Catal., A* **2004**, *274*, 229.
29. Xingyi, W.; Qian, K.; Dao, L.; *Appl. Catal., B* **2009**, *86*, 166.
30. Arena, F. G.; Trunfio, G.; Negro, J.; Spadaro, L.; *Appl. Catal., B* **2008**, *85*, 40.
31. Töpfer, J.; Feltz, A.; Gräf, G.; Hackl, B.; Raupach, L.; Weissbrodt, P.; *Phys. Status Solidi A* **1992**, *134*, 405.
32. Huang, Z.; Zhou, W.; Ouyang, C.; Wu, J.; Zhang, F.; Huang, J.; Chu, J.; *Sci. Report* **2015**, *5*, 10899.
33. Rao, T.; Shen, M.; Jia, L.; Hao, J.; Wang, J.; *Catal. Commun*. **2007**, *8*, 1743.
34. Bensalem, A.; Bozon-Verduraz, F.; Delamar, M.; Bugli, G.; *Appl. Catal., A* **1995**, *121*, 81.
35. Holgado, J. P.; Munuera, G.; Espinós, J. P.; Gonzalez-Elipe, A. R.; *Appl. Surf. Sci.* **2000**, *158*, 164.
36. Deng, W.; Dai, Q.; Lao, Y.; Shi, B.; Wang, X.; *Appl. Catal., B* **2016**, *181*, 848.
37. Wu, M.; Wang, X.; Dai, Q.; Gu, Y.; Li, D.; *Catal. Today* **2010**, *158*, 336.
38. Burroughs, P.; Hamnett, A.; Orchard, A. F.; Thornton, G.; *J. Chem. Soc.* **1976**, *17*, 1686.
39. Bêche, E.; Charvin, P.; Perarnau, D.; Abanades, S.; Flamant, G.; *Surf. Interface Anal.* **2008**, *40*, 264.
40. Romeo, M.; Bak, K.; El Fallah, J.; Le Normand, F.; Hilaire, L; *Surf. Interface Anal.* **1993**, *20*, 508.
41. Fujimori, A.; *Phys. Rev. B* **1983**, *28*, 2281.
42. Seah, M. P. In *Practical Surface Analysis*; Briggs, D., Seah, M. P., eds.; John Wiley & Sons: Chichester. 1983, ch. 1.
43. Paparazzo, E.; *Superlattices Microstruct.* **2017**, *105*, 216.
44. Si, W.; Wang, Y.; Peng, Y.; Li, X.; Li, K.; Li, J.; *Chem. Commun.* **2015**, *51*, 14977.